2006

# Thermal Desorption of Hydrogen from Carbon Nanosheets

X. Zhao

R. A. Outlaw

J. J. Wang

M. Y. Zhu

Gregory D. Smith
*William & Mary*, gdsmit@wm.edu

*See next page for additional authors*



## Recommended Citation

Zhao, X.; Outlaw, R. A.; Wang, J. J.; Zhu, M. Y.; Smith, Gregory D.; and Holloway, B. C., Thermal Desorption of Hydrogen from Carbon Nanosheets (2006). *The Journal of Chemical Physics*, 124. https://doi.org/10.1063/1.2187969

# Thermal desorption of hydrogen from carbon nanosheets

X. Zhao, R. A. Outlaw, J. J. Wang, M. Y. Zhu, G. D. Smith, and B. C. Holloway[a)]
*Department of Applied Science, College of William and Mary, Williamsburg, Virginia 23187-8795*

(Received 14 December 2005; accepted 23 February 2006; published online 16 May 2006)

Carbon nanosheets are a unique nanostructure that, at their thinnest configuration, approach a single freestanding graphene sheet. Temperature desorption spectroscopy (TDS) has shown that the hydrogen adsorption and incorporation during growth of the nanosheets by radio frequency plasma-enhanced chemical vapor deposition are significant. A numerical peak fitting to the desorption spectra (300–1273 K) via the Polanyi-Wigner equation showed that desorption followed a second order process, presumably by the Langmuir-Hinshelwood mechanism. Six peaks provide the best fit to the TDS spectra. Surface desorption activation energies were determined to be 0.59, 0.63, and 0.65 eV for the external graphite surface layers and 0.85, 1.15, and 1.73 eV for desorption and diffusion from the bulk. In contrast to TDS data from previously studied *a*-C:H films [Schenk *et al.* J. Appl. Phys. **77**, 2462 (1995)], a greater amount of hydrogen bound as $sp^2$ hybridized carbon was observed. A previous x-ray diffraction study of these films has shown a significant graphitic character with a crystallite dimension of $L_a=10.7$ nm. This result is consistent with experimental results by Raman spectroscopy that show as-grown carbon nanosheets to be crystalline as commercial graphite with a crystallite size of $L_a=11$ nm. Following TDS, Raman data indicate that the average crystallite increased in size to $L_a=15$ nm. © *2006 American Institute of Physics*. [DOI: 10.1063/1.2187969]

## INTRODUCTION

Vertically oriented and freestanding carbon nanosheets of 1–7 graphene layers thick have been synthesized via radio frequency plasma-enhanced chemical vapor deposition (rf PECVD).[1,2] This new morphological structure of carbon-based materials has great promise in a number of applications. For example, as a cold cathode electron field emission source, the very thin edges (<1 nm) of the sheets provide the high field enhancement factor ($\beta$) necessary to promote tunneling and the corresponding electron emission.[3] Further, the high specific surface area of the films suggests potential applications for hydrogen storage and catalyst support structure for fuel cells. The growth environment, a $CH_4/H_2$ plasma, generates hydrogen atoms and ions that are readily adsorbed and incorporated into the films. The high energy of the plasma produces defects that affect the growth mechanism as well as the physical properties of the film. It is the purpose of this paper to measure the quantity of absorbed hydrogen and to determine the partitioning and site locations of the H atoms in the carbon nanosheets via thermal desorption spectroscopy (TDS).

## EXPERIMENTAL METHODS

Carbon nanosheets (CNSs) were deposited on clean, vacuum annealed $4\times4\times0.075$ mm$^3$ tantalum substrates. The growth parameters were 40% $CH_4$/60% $H_2$ at $p\sim0.1$ Torr and an rf power of 900 W. A thorough description of the inductively coupled rf PECVD growth system and characterization of this material have been presented elsewhere.[2–5]

*Ex situ* characterization was completed using a Hitachi S-4700 scanning electron microscope operating at a beam voltage of 15 kV and a beam current of 10 $\mu$A for morphology imaging and a Renishaw™ inVia™ micro-Raman (514 nm) for crystalline measurements. For the Raman study, three samples were tested as received and after TDS, respectively.

Scanning electron microscopy (SEM) shows the vertically oriented freestanding films to be approximately 1–2 nm thick and 600 nm high. A high-resolution transmission electron microscopy (HRTEM) study[1] demonstrated that there are approximately 1–7 layers of graphene planes that make up the individual sheet, often terminated with edges of 1–3 graphene layers. Rhenium wires (0.125 mm diameter) were spot welded to the Ta substrates for resistive heating from room temperature up to 1000 °C. Individual samples were admitted into the preparation chamber ($p\sim1\times10^{-8}$ Torr), heated to 150 °C for 1 h to remove water, then transferred into the surface analysis chamber ($p<1\times10^{-10}$ Torr) for testing.

The analysis chamber is equipped with angle resolved Auger electron spectroscopy (ARAES), angle resolved x-ray photoelectron spectroscopy (ARXPS), and temperature desorption spectroscopy (TDS). The sample was positioned on a carousel station to which power could be provided. The sample was rotated and positioned in front of the cylindrical mirror analyzer for selected surface analysis or on axis with the ion source of an SRS RGA100™ quadrupole mass spectrometer (QMS) for TDS. The ion source of the mass spec-

[a)]Electronic mail: holloway@as.wm.edu

 

trometer was encapsulated with an Au coated quartz envelope fashioned with a 5 mm aperture on the axis to minimize background effects and enhance spectral resolution.[6] The RGA was mounted on a linear motion feedthrough that facilitates the ion source to approach within 1 mm of the sample. The plane of the Ta substrate and the entrance aperture were in a parallel-plane geometry. Auger spectra of the CNS showed a perfect graphite peak and no contamination.

An iris valve within the surface analysis system was adjusted to throttle the pumping speed, the minimum of which for $H_2$ is 88 l/s with the orifice diameter of 6 mm. A customized LABVIEW™ program monitored the partial pressure of various gas species in real time. The program synchronized the pressure signals from the QMS, and the current/temperature to the carbon nanosheets. A second customized LABVIEW™ program was used to record and plot the spectra.

The partial pressure and TDS desorption rate are related as

$$-V\frac{dp}{dt}+Q=Sp, \tag{1}$$

where $Q$ is the mass flow rate of desorption, $S$ is the pumping speed, $p$ is the pressure, and $V$ is the volume of the surface analysis chamber. With the iris valve fully open, the pumping speed $S$ (l/s) to volume ratio is so large that $dp/dt \ll (S/V)p$; therefore the contribution of $-V(dp/dt)$ can be ignored.[7] Equation (1) is therefore reduced to

$$Q \approx Sp. \tag{2}$$

For a single desorption energy, the $H_2$ desorption process follows the Polanyi-Wigner equation.[8] The desorption rate $r(\theta)$ is given by

$$r(\theta)=-\frac{d\theta}{dt}=\nu\theta^2\exp\left(-\frac{\Delta E_d}{kT}\right), \tag{3}$$

where $k$ is Boltzmann's constant, $\Delta E_d$ is the activation energy of desorption, $t$ is the time, $T$ is the temperature in Kelvin, $\theta$ is the adsorbate fractional coverage, $-d\theta/dt$ is the desorption rate and $\nu$ is the preexponential factor. The physical meaning of $\nu$ is generally related to the adatom vibration frequency on the surface. Combining Eqs. (1)–(3), the partial pressure $(p_i)$ and adsorbate fractional coverage $(\theta)$ of a species are related as

$$p_i=CN_i\left(-\frac{d\theta_i}{dt}\right), \tag{4}$$

where $N_i$ is the total number of adatoms which diffuse and recombine with the same desorption activation energy $\Delta E_{d,i}$, and $C$ (Torr s) is a constant. For the convenience of numeric computation, $p_{\text{total}}$ was scaled by a constant $K$ to arbitrary units $p^*_{\text{total}}$, where the maximum value of $p^*_{\text{total}}$ is set at 1000. The relationship between time $(t)$ and temperature is

$$T=300+\alpha t\ (\text{K}), \tag{5}$$

where $\alpha$ is the temperature ramp rate. Combining Eqs. (3)–(5),

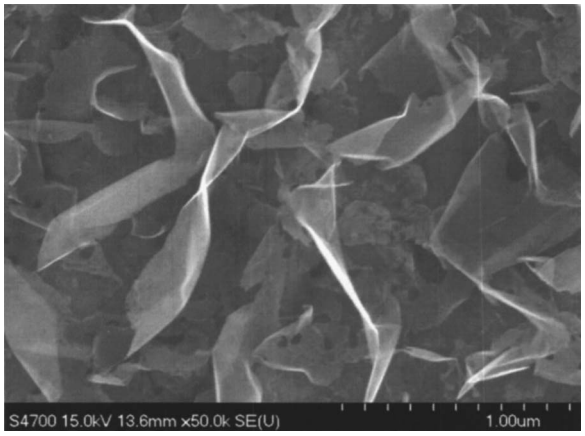


FIG. 1. SEM image of carbon nanosheets, grown on Ta substrate, shown after TDS (plan view). The plan view image shows the random orientation and corrugated nature of the nanosheets. Compared to as-received nanosheets, there is no change in morphology.

$$p^*_{\text{total}}(T)=\left(\frac{KC}{\alpha}\right)\sum_i N_i\nu_i\theta_i^2\exp\left(-\frac{\Delta E_{d,i}}{kT}\right), \tag{6}$$

where $K$, $C$, and $\alpha$ are the constants in the equation. $N_i$, $\nu_i$, and $\Delta E_{d,i}$ are the key parameters with specific physical meanings as mentioned.

In previous research of Jong and Niemantsverdret,[8] eight different methods have been suggested to evaluate the desorption parameters, $N$, $\nu$, and $\Delta E_d$, from TDS spectra. However, none of them can adequately solve multipeak spectra from a second order process. For instance, if the peak temperature $T_m$ is known, the desorption energy $\Delta E_d$ can be easily found by *Redhead's* peak maximum formula

$$\Delta E_d=RT_m[\ln(\upsilon T_m/\alpha)-3.46], \tag{7}$$

where $\alpha$ is the same as Eq. (5). But this equation is only valid for first order desorption processes and has to assume $\nu/\alpha$ as a constant.

To resolve multipeaks in empirical TDS spectrum, several researchers[9] utilized Gaussian curves to deconvolute data. However, this method does not accurately account for the kinetic process of desorption, which is conventionally depicted by the Polanyi-Wigner equation.[8]

In this study, a MATLAB™ program was developed to fit the empirical multipeak TDS spectrum $(p^*_{\text{total}})$ with a set of parameters ($N_i$, $\nu_i$, and $\Delta E_{d,i}$) in Eq. (6). The program's algorithm is to use the sum of a series of independent Polanyi-Wigner equations to simulate empirical data. This method is consistent with Su and Lin's[10] work that used a similar algorithm to simulate two-peak empirical TDS spectra. Our program in MATLAB™ scripts can be found on AIP's Electronic Physics Auxiliary Publication Service (EPAPS) website free of charge.[27]

## RESULTS

Figure 1 is an SEM of a nanosheet sample after TDS. The plan view image shows the random orientation and corrugated nature of the nanosheets. Compared to as-grown nanosheets,[1,2] there is no visible change in the morphology from the SEM following TDS (up to 1273 K). Figure 2 is a

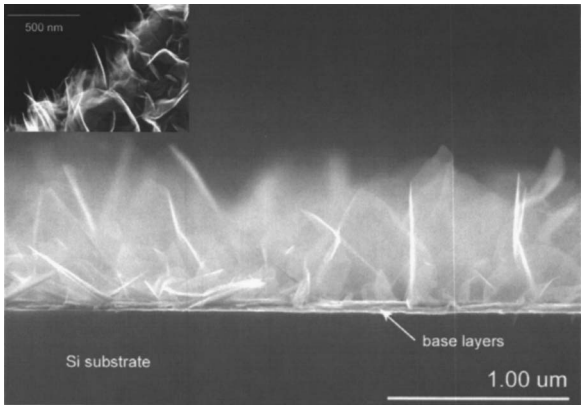


FIG. 2. SEM image of carbon nanosheets grown on Si substrate (cross-section view) which has been cleaved to show the base layers of carbon below the nanosheets. The vertically oriented freestanding films are approximately 1–2 nm thick and 600 nm high.

cross-section view of a nanosheet sample grown on a Si substrate, which has been cleaved to show the bulk layers of carbon below the nanosheets.

Raman spectra of the CNS, before and after TDS, are shown in Fig. 3. The initial $D(1356\ \mathrm{cm}^{-1})/G(1581\ \mathrm{cm}^{-1})$ ratio is ~0.39, but this decreased to 0.29, or about a 25% decrease after the vacuum annealing or TDS experiments to 1273 K.

TDS spectra were run at temperature ramp rates of $\alpha = 25$, 20, 15, 10, and 5 K/s to find the optimum resolution. For each ramp rate, TDS was repeated with three samples. Figure 4 shows comparative data at $\alpha = 25$, 20, and 15 K/s (the slower ramp rates of 10 and 5 had poor resolution and are not shown to retain figure clarity). Positioning the sample 5 mm from the entrance aperture of the quartz envelope of the QMS in a parallel-plane geometry and applying $\alpha = 15$ K/s yielded the best resolution.

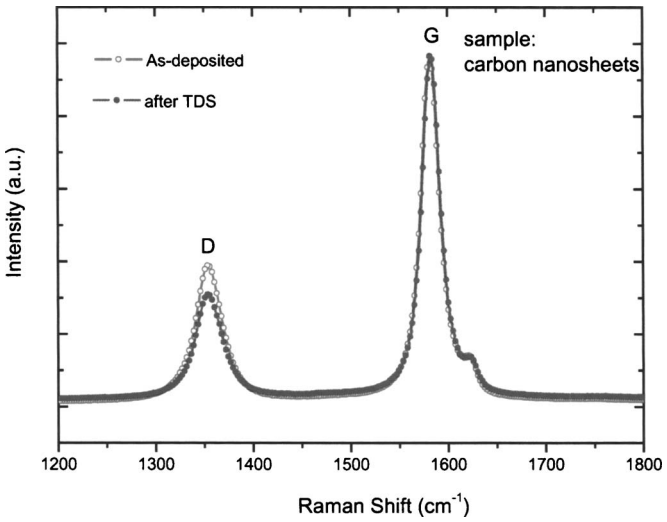


FIG. 3. Raman spectra of carbon nanosheets before and after TDS experiment. The $D$ (1356 $\mathrm{cm}^{-1}$)/$G$ (1581 $\mathrm{cm}^{-1}$) ratio of the as-deposited material was ~0.39. The $D/G$ ratio decreased to ~0.29 after vacuum annealing (1273 K) or TDS experiments (1273 K), indicating an increasing order and grain growth in the material which we attribute to carbon relaxation and recovery due to removal of adsorbed hydrogen.

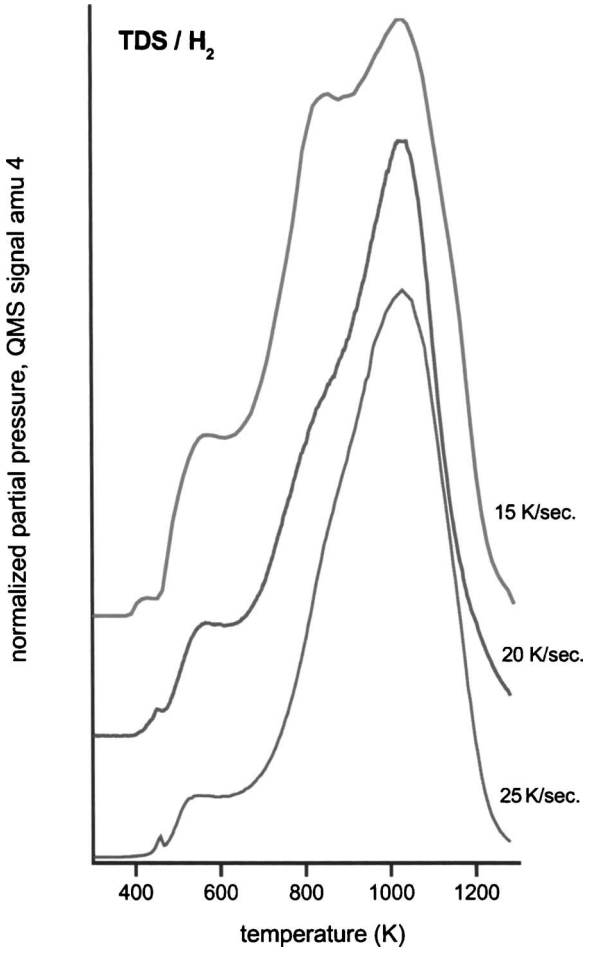


FIG. 4. $H_2$ TDS spectra from carbon nanosheet samples at temperature ramp rates ($\alpha$) of 25, 20, and 15 K/s. A ramp rate of 15 K/s yielded the best resolution and was used for numerical peak fitting. Spectra collected at $\alpha = 10$ and 5 K/s did not yield adequate resolution and are not shown for clarity.

The total amount of H atoms released ($N_{\mathrm{total}}$) is related to the pressure ($p$) by

$$N_{\mathrm{total}} = \frac{2S}{kT_{\mathrm{room}}} \int_0^\infty p dt. \tag{8}$$

The average number of H adatoms released from a $4 \times 4\ \mathrm{mm}^2$ carbon nanosheet sample was $\sim 3.8 \times 10^{16}$ at. (±5% over three samples). The precise weight of the carbon nanosheet sample is so small that an accurate measurement is difficult, but a rough estimate indicates 0.02 $\mathrm{mg/cm}^2$, which equals to 1 H atom for every 4.5 C atoms.

Figure 5 shows repeatable and representative TDS at $\alpha = 15$ K/s. According to our TDS experimental setup and results, C equals $10^{-20}$ Torr/s and K equals $1.2 \times 10^9\ \mathrm{Torr}^{-1}$. The experimental data were fitted by numerically integrating Eq. (3) by assuming $n$ subpeaks and thus $n \times 3$ initial estimates. The minimum number of subpeaks to give the best quality of fit was found to be 6. The resulting curves were summed following Eq. (6) and compared to the experiment spectra to give a root mean squared error of fit. Subsequent Brownian random search resulted in the best-fit parameters shown in Table I with the least root mean square error of 0.3%. The only good fit to the data was a second order pro-

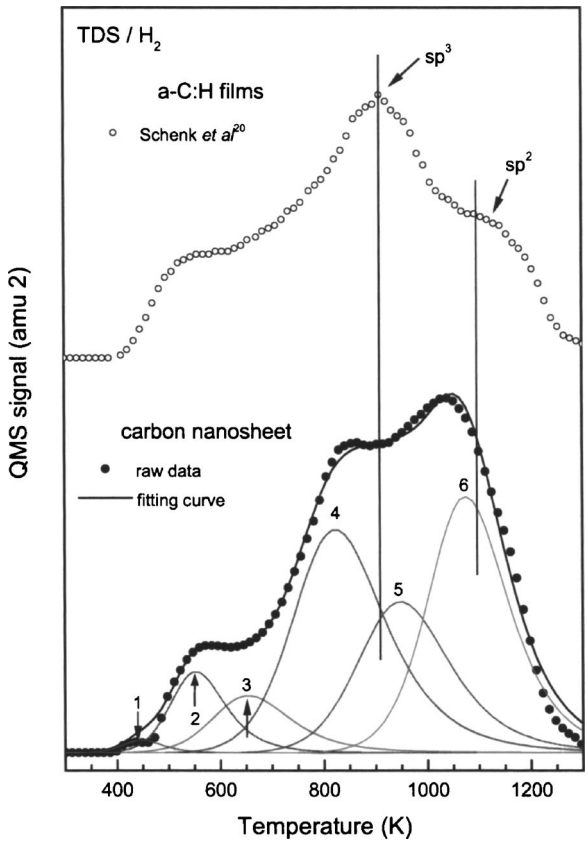


FIG. 5. $H_2$ TDS spectra of carbon nanosheets ($\alpha$=15 K/s) with the corresponding subpeaks from a numerical integration of the second order desorption equations. The minimum number of subpeaks required to produce the best fit was 6. Fitting parameters are presented in Table I. Previously published amorphous carbon film data from Schenk *et al.* (Ref. 18) are also presented for comparison.

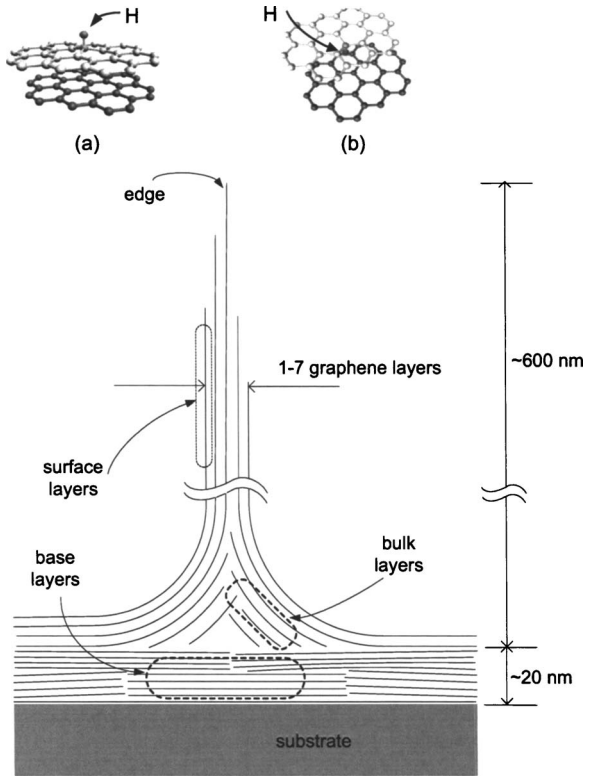


FIG. 6. A schematic of idealized carbon nanosheets shows the edges, surface layers, bulk, and base layers. The majority of $H_2$ comes from recombination, diffusion, and desorption from the bulk layers. Inset (a) is a schematic representation of a hydrogen atom adsorbed in an outward configuration on a graphitic surface. Inset (b) is a schematic representation of a hydrogen atom absorbed in an interior configuration on a graphitic surface.

cess ($n$=2), which represents recombination of H atoms before they leave the surface. The data from the numerical fit for the peaks $i$=1–6 are shown in Table I.

The preexponential values required for the least rms fit vary from $10^{4.28}$ to $10^{7.56}$ 1/s for the specific hydrogen bond, which is much lower than the conventional assignment of $10^{12}$–$10^{14}$ 1/s usually applied in TDS analysis. This is not without precedent, however. Recently, several authors have suggested an electron transition component in addition to the vibrational energy transfer and reported values of $\nu$ in the $10^4$–$10^6$ 1/s range.[11]

The integration of the individual peaks shown in Fig. 5 yields a concentration from the bulk layers five times greater than the surface (see Table I). Further, during the TDS process, no atomic H was detected; only $H_2$ and negligible amounts (<0.1%) of other desorbed gases were observed. Since the partial pressure of background gas-phase $H_2$ is negligible ($p \sim 1 \times 10^{-10}$ Torr), impingement of hydrogen on the surface is also negligible. Therefore, recombination by the Eley-Rideal[12,13] (ER) mechanism is highly unlikely, i.e., H from the gas phase combining with H adsorbed on the surface. Conversely, the Langmuir-Hinshelwood[12,13] (LH) mechanism is a more likely explanation for the observed TDS kinetics, i.e., H adatoms diffuse on the surface, collide, and recombine to $H_2$ before desorption.

TABLE I. Parameters calculated from the TDS data using Eqs. (3) and (6).

| Peak $i$ | $\log_{10}(N_i)$ | $\log_{10}(\nu_i)$ | $\Delta E_{d,i}$ (eV) | $T_{\text{peak}}$ (K) | $\left(\frac{N_i}{\Sigma_i N_i}\right)\times 100\%$ |
|---|---|---|---|---|---|
| 1 | 14.47 | 6.38 | 0.596 | 445 | 0.78 |
| 2 | 15.42 | 5.56 | 0.653 | 550 | 6.87 |
| 3 | 15.39 | 4.28 | 0.636 | 650 | 6.86 |
| 4 | 16.08 | 4.50 | 0.847 | 820 | 31.91 |
| 5 | 15.91 | 5.48 | 1.15 | 948 | 21.42 |
| 6 | 16.08 | 7.56 | 1.73 | 1080 | 31.63 |

## DISCUSSION

The growth of the CNS by inductively coupled rf PECVD with 40% $CH_4/H_2$ at ~0.1 Torr and $T \sim 680$ °C generates a sheet growth rate of ~0.5 nm/s. The thickness of the sheets varies from 1 to 7 graphene layers with termination edges of 1–3 graphene layers.[5] A schematic representation of an individual sheet is shown in Fig. 6. The high-energy plasma necessary to grow the ultrathin sheets is also likely to generate a significant defect density as well as adsorb/incorporate many hydrogen atoms. The Raman spectra shown in Fig. 3 show a $D/G$ ratio of ~0.39 for representative as-grown CNS, which is very similar to that determined by Tuinstra and Koening[14] for commercial grade graphite (~0.39). The structure of the CNS, after vacuum annealing (1273 K for 10 min) or after a TDS run

(300–1273 K) for ~2 min, showed no apparent morphology change when observed by SEM, but the $D/G$ ratio decreased to ~0.29. This decrease in the $D/G$ ratio may also be connected with desorbed hydrogen since H atoms can induce tetragonalization (puckering) of the C atoms in the graphene plane.[13,15,16] Hydrogen adatom removal should promote planar relaxation back to a more ordered condition and allow vacated carbon atoms (previously H terminated) to mend and grow the graphene lattice. This is consistent with the work of Schenk *et al.*,[17,18] Biener *et al.*,[19,20] and Zecho *et al.*;[21] electron energy loss spectroscopy (EELS) and high-resolution electron energy loss spectroscopy (HREELS) of *a*-C:H films taken after annealing show a substantial shift towards $sp^2$ graphitization. The $\pi$ plasmon was observed to shift over 1.5 eV to plasmon energy of 6.5 eV when the hydrogen was desorbed. This $\pi$ plasmon energy is characteristic of pure graphite.[19,21] The carbon nanosheet films studied in this work are more graphitic than the *a*-C:H films of Schenk *et al.*, Biener *et al.*, or Zecho *et al.* and appear to have adsorbed/incorporated far less hydrogen in the growth process. The x-ray diffraction (XRD) measurements[5] of similar nanosheet samples have shown a significant graphitic character with a crystallite dimension of $L_a=10.7$ nm. The Raman data in Fig. 3 of the as-deposited CNS indicate a narrow full width at half maximum (FWHM) for the $G$ peak of $\Delta W_G=21\ \mathrm{cm}^{-1}$. Figure 6 indicates that the intensity ratio of the $D/G$ peak is 0.39. Using the empirical formula $L_a=4.4/(I_D/I_G)$ nm in the work of Kurita *et al.*,[22] the average crystallite diameter for the ordered grains is 11.3 nm which is in excellent agreement with the XRD measurements. A similar calculation for the Raman data after TDS gives a crystallite growth to $L_a=15$ nm.

Since we have limited our TDS to 1273 K and since some C–H covalent bonds[23] have been calculated to be in excess of 4.8 eV (e.g., on the edges), it is probable that not all the adsorbed hydrogen has been desorbed. This is also consistent with other researchers' observations that 2800 K is necessary to completely desorb all hydrogen.[24] Peak fitting of the TDS spectrum, presented in Fig. 5, shows six significant subpeaks. The position of first two peaks (1, 2) at about 445 and 550 K are in good agreement with the experimental data reported by Zecho *et al.*,[15] for H atom adsorption on highly oriented pyrolytic graphite (HOPG) surface. Our interpretation is that the H atoms/ions are adsorbed on the available in-plane sites of the C atoms, which are located on the surface layers of the nanosheets. Figure 6 is an illustration of nanosheets showing the zones of edges, surface layers, and bulk layers. Specifically, the sites can be assigned to peaks 1-2 on the top of surface C atoms projecting outward [Figure 6 inset (a)] and/or on subsurface C atoms projecting into the space between graphene layers [Fig. 6 inset (b)]. It is known that half of the C atoms in the graphite lattice align on top of each other with a distance of $c/2$ in the $z$ direction (C1 sites) and the other half align above the centers of the six-member ring of the adjacent graphene planes (C2 sites).[16] In the case shown in inset (a), H could be adsorbed on either C1 or C2 sites. However, in the case shown inset (b), the attached C atoms could be only in C2 sites, where the H atoms are also centered within the adjacent surface (or bulk) hexagonal rings. In both cases, the hydrogen is bonded to the surface C atoms in an $sp^3$ hybridization fashion and causes lattice distortion (tetragonalization). The activation energy for the 445 K peak was found to be 0.6 eV (correction for zero point energy gives a computed value of 0.83 eV). Our measurements of 0.59 and 0.65 eV on the peak 1 (445 K) and peak 2 (550 K), respectively (zero point energy neglected), are close to the density functional calculations of Ferro *et al.*[12,13] and Zecho *et al.*[15] Due to its similar activation energy of 0.639 eV, peak 3 (660 K) could also be assigned to the same group of H adsorbates. Based on the area fraction of peaks 1, 2, and 3, 16% of the total $H_2$ desorbed from the CNS appears to have desorbed from the surface.

The high temperature peaks (4, 5, and 6) observed at 820, 948, and 1080 K indicate a concentration six times greater than that of the low temperature peaks. These peaks most likely represent H atoms adsorbed on sites within the bulk. The mechanism for desorption of these H atoms is either by interplanar diffusion of atomic H and surface recombination or by atomic H recombination and $H_2$ molecule diffusion directly between the layers to the external surface. Normal (orthogonal) atomic diffusion through the layers has a very high activation barrier of 4.13 eV,[12] so, of course, is far less probable. In Fig. 5, the data of Schenk *et al.*[18] for TDS from *a*-C:H film have been plotted to compare to the data in this work. The overall TDS spectra are quite similar. Peak 4 at 820 K in our work can be compared with the major peak at 920 K in the work of Schenk *et al.* which they attribute to $sp^3$ hybridized $CH_x$ ($x=1-3$). In the –CH configuration, one H atom is bound to an $sp^3$ hybridized C, which connect to three adjacent C atoms. In the $–CH_2$ configuration, H atoms are bound to an $sp^3$ hybridized C, which could connect to two adjacent C atoms. In the $–CH_3$ configuration, H atoms bound to one $sp^3$ hybridized C, could only connect to one adjacent C atom. The difference in the peak temperatures of desorption in our work compared to the work of Schenk *et al.* on *a*-C:H films may be attributed to the differences in diffusion and recombination from between the planes of the more ordered graphitic structure compared to an amorphous material. For the peak temperature deviation, another possible reason probably is the concentration difference on $sp^3$ hybridized $CH_x$ ($x=1-3$) groups in carbon nanosheets and *a*-C:H films, respectively. Carbon nanosheets have long-range ordered graphitic structure ($L_a\sim 10$ nm). Therefore, this structure is unlikely to accommodate large populations of the three dimensional $–CH_2$ and $–CH_3$ bonds in the graphene plane except at the crystal boundaries. In our work, the hydrocarbon gases desorbed were negligible ($<1\%$) which suggests that the desorbed hydrogen is more likely coming from the aforementioned tetrahedral –CH bonding to the C2 sites[16] within the bulk.

Peak 6 at 1080 K can be compared to the peak of Schenk *et al.* at 1150 K to which they attribute to $sp^2$ hybridized $CH_x$ ($x=1-2$). As previously indicated by XRD (Ref. 5) and Raman spectroscopy, the nanosheets are much more graphitic than the *a*-C:H films of Schenk *et al.*,[17,18] Biener *et al.*,[19,20] Zecho *et al.*,[21] and the work of Wild *et al.*[25] and, as such, peak 6 should be dominant in the nanosheet spectra. Hydrogen bound to carbon in the $sp^2$ hybridized

bond most likely is at the crystal boundaries where dangling bonds, vacancies, pentagon, and network disorder allow a C–H structure to be accommodated. Peak 5 is not obvious but is necessary to obtain a close fit consistent with the Polanyi-Wigner equation. A possible explanation for this TDS peak is hydrogen bonding on the C atoms of mixed $sp^2/sp^3$ hybridization, which occurs at defects in the bulk, such as Stone-Wales defects.[16,26] Desorption activation energies determined for the high-energy peaks found in our work are 0.85, 1.15, and 1.7 eV. Since no atomic hydrogen is detected in our TDS experiment, the energies represent the activation barriers to interplanar diffusion and/or recombination, which are the two rate-limiting steps to molecular desorption.

Ferro *et al.* make a compelling case for surface recombination consistent with the Langmuir-Hinshelwood mechanism.[13] Their calculations suggest a 1.25 eV barrier to migration of an isolated H atom, a 0.46 eV diffusion barrier in the vicinity of another H adatom, and a 2.72 eV rate-limiting barrier to recombination (when the two H atoms are less than a C–C bond length), all on a free graphene surface. This last activation barrier is considerably higher than even the highest desorption energy (1.7 eV) determined in this work, suggesting that this is not the primary bulk desorption mechanism in nanosheets.

The normal interplanar spacing of graphite is[16] $d=0.334$ nm, and the graphene layers studied in this work have an even larger separation[5] ($d=0.34$ nm) because of the reduction in $c$-axis confinement due to the lack of long-range forces. The nanosheet interplanar distance is substantially greater than the $H_2$ molecular diameter of 0.271 nm, which suggests that recombination may occur between the graphene layers because $H_2$ has room to diffuse as a molecule.

## CONCLUSIONS

Temperature desorption spectroscopy of carbon nanosheets grown by rf PECVD in a $CH_4/H_2$ plasma has shown surface and bulk desorption peaks from the recombination of hydrogen atoms by the Langmuir-Hinshelwood mechanism. Resolution of the peaks was accomplished by numerical fit to the Polanyi-Wigner equation. The ratio of the bulk to surface concentration was found to be $\sim 6/1$. The surface desorption activation energy of 0.59 eV has been favorably compared to several density functional calculations reported in literature.[12,13,15] Comparison of the carbon nanosheet data to $a$-C:H films from other research[17,18] shows similar TDS spectra, but with a greater hydrogen bonding to $sp^2$ hybridized carbon than $sp^3$ hybridized carbon. This is expected since the carbon nanosheets are far more graphitic than the amorphous films. The graphitic character is confirmed by XRD and Raman spectroscopy which give $L_a \sim 11$ nm. Raman spectroscopy also showed a 25% crystallite increase in the carbon nanosheets after TDS. This grain growth has been interpreted as a combination of the removal of the hydrogen, which permits surface relaxation, recovery, and thermal ordering of the nanosheets. Finally, since the C–H bonding energy on the edge of the graphene sheet has been calculated as high as 4.8 eV and substrate temperature as high as 3000 K is needed for complete hydrogen removal, it is probable that this TDS work does not include edge-bonded hydrogen.


[1] J. J. Wang, M. Y. Zhu, R. A. Outlaw, X. Zhao, D. M. Manos, and B. C. Holloway, Appl. Phys. Lett. **85**, 1265 (2004).
[2] J. J. Wang, M. Zhu, R. A. Outlaw, X. Zhao, D. M. Manos, and B. C. Holloway, Carbon **42**, 2867 (2004).
[3] J. J. Wang, M. Zhu, X. Zhao, R. A. Outlaw, D. M. Manos, B. C. Holloway, C. Park, T. Anderson, and V. P. Mammana, J. Vac. Sci. Technol. B **22**, 1269 (2004).
[4] J. J. Wang, M. Zhu, R. Outlaw, X. Zhao, D. M. Manos, B. B. Holloway, V. Mammana, M. Ray, and J. Dalton, presented at the Technical Digest of the 17th International Vacuum Nanoelectronics Conference, Piscataway, NJ, 2004 (unpublished), IEEE Catalog No. 04TH8737, pp. 222–22.
[5] B. L. French, J. J. Wang, M. Y. Zhu, and B. C. Holloway, J. Appl. Phys. **97**, 114317 (2005).
[6] P. Feulner and D. Menzel, J. Vac. Sci. Technol. **17**, 662 (1980).
[7] D. A. King, Surf. Sci. **47**, 384 (1975).
[8] A. M. d. Jong and J. W. Niemantsverdret, Surf. Sci. **233**, 355 (1990).
[9] L. D. Lopez-Carreno, A. J. Ramirez-Cuesta, L. Viscido, and J. M. Heras, J. Mol. Catal. A: Chem. **167**, 157 (2001); L. D. Lopez-Carreno, J. M. Heras, and L. Viscido, Surf. Sci. **377–379**, 615 (1997); W. Lisowski, E. G. Keim, A. H. J. v. d. Berg, and M. A. Smithers, Carbon **44**, 974 (2006).
[10] C. Su and J. C. Lin, Surf. Sci. **406**, 149 (1998).
[11] A. A. Hassz, P. Franzen, J. W. Davis, S. Chiu, and C. S. Pitcher, J. Appl. Phys. **77**, 66 (1994); B. R. Trenhaile, V. N. Antonov, G. J. Xu, K. S. Nakayama, and J. J. Weaver, Surf. Sci. **583**, 135 (2005); R. J. Hamers, Surf. Sci. **583**, 1 (2005).
[12] Y. Ferro, F. Marinelli, and A. Allouche, J. Chem. Phys. **116**, 8124 (2002).
[13] Y. Ferro, F. Marinelli, and A. Allouche, Chem. Phys. Lett. **368**, 609 (2003).
[14] F. Tuinstra and J. L. Koenig, J. Chem. Phys. **53**, 1126 (1970).
[15] T. Zecho, A. Guttler, X. Sha, B. Jackson, and J. Kuppers, J. Chem. Phys. **117**, 8486 (2002).
[16] S. Letardi, M. Celino, F. Cleri, and V. Rosato, Surf. Sci. **496**, 33 (2002).
[17] A. Schenk, J. Biener, B. Winter, C. Lutterloh, U. A. Schubert, and J. Kuppers, Appl. Phys. Lett. **61**, 2414 (1992).
[18] A. Schenk, B. Winter, J. Biener, C. Lutterloh, U. A. Schubert, and J. Kuppers, J. Appl. Phys. **77**, 2462 (1995).
[19] J. Biener, A. Schenk, B. Winter, U. A. Schubert, C. Lutterloh, and J. Kuppers, Phys. Rev. B **49**, 17307 (1994).
[20] J. Biener, A. Schenk, B. Winter, C. Lutterloh, U. A. Schubert, and J. Kuppers, Surf. Sci. Lett. **291**, L725 (1993).
[21] T. Zecho, B. D. Brandner, J. Biener, and J. Kuppers, J. Phys. Chem. B **105**, 6194 (2001).
[22] S. Kurita, A. Yoshimura, H. Kawamoto, T. Uchida, K. Kojima, and M. Tachibana, J. Appl. Phys. **97**, 104320 (2005).
[23] K. May and S. Dapprich, Phys. Chem. Chem. Phys. **2**(22), 5084 (2000); K. May and R. Ahlrichs, *ibid.* **2**(22), 5089 (2000).
[24] M. S. Dresselhous and P. Eklund, *Science of Fullerenes and Carbon Nanotubes* (Academic Press, New York, 1996), p. 15.
[25] C. Wild and P. Koidl, Appl. Phys. Lett. **51**, 1506 (1987).
[26] E. J. Duplock, M. Scheffler, and P. J. D. Lindan, Phys. Rev. Lett. **92**, 225502 (2004).
[27] See EPAPS Document No. E-JCPSA6-124-701614 for the authors' MATLAB™ script. This document can be reached via a direct link in the online article's HTML reference section or via the EPAPS homepage (http://www.aip.org/pubservs/epaps.html).